CrossMark

ORIGINAL ARTICLE

A Simple Analysis of Reinforced Soil Using Equivalent Approach

V. B. Maji[1] · V. S. Sowmiyaa[1] · R. G. Robinson[1]

Abstract Equivalent approach to analyse reinforced soil has an advantage that the study of complex interaction between the soil and reinforcement is avoided and the stress–strain characteristics are obtained similar to a homogeneous material. Present study aims to investigate the behaviour of reinforced soil structures by considering it as an equivalent medium with homogeneous properties. A numerical model is developed using *FLAC* and is systematically verified using extensive laboratory test results of large diameter triaxial tests. The developed model is also compared with discrete approach, where the reinforcement layers are explicitly modelled. The developed equivalent model could capture the strength and deformation behaviour of the reinforced sand and the failure mechanisms quite well. Model is later extended to analyse two case studies on reinforced retaining walls using the properties adopted from the literature. The results from the equivalent analysis were verified with instrumented data together with discrete numerical approach.

Keywords Reinforced soil · Equivalent approach · Numerical model · *FLAC* · Retaining wall

Introduction

The reinforced soil structures are advantageous than the conventional structures, due to their simplicity and faster construction. Though the reinforced soil concepts were in use since ancient times, modern use of soil reinforcing technique was first pioneered by the French Engineer, Henri Vidal. The first major work on reinforced earth was introduced from 1964 onwards in both USA and Europe. The first use of geotextiles in soil reinforcement was started in 1971 in France for the construction of embankments over weak subgrades. In the last few decades, there is tremendous progress in the reinforced earth domain with the use of many different types of reinforcements like strips, grids and sheets. The composite behaviour of this reinforced earth depends on the interaction between the soil and the material. The discrete approach to model reinforced soil structures becomes quite complex since modelling each component and their interactions becomes tedious and time consuming. Moreover, modelling the interface between the soil and the reinforcement is challenging. In the equivalent approach, the composite reinforced soil properties are considered together and hence less number of input parameters are needed to develop the numerical model. The numerical model becomes simple and much easier than discrete elements with less computation time. However, the disadvantage is that the localized failure cannot be modelled, as the individual material properties are not used and the interaction between the soil and the reinforcement cannot be studied independently.

In the discrete method, the soil is usually modeled using some elasto-plastic, linear elastic or non-linear models where as the reinforcements are generally treated as linear elastic materials. The interface between the soil and the reinforcement are generally modelled by two approaches, the constraint approach and contact elements. In constraint approach, separation is not allowed between the soil and the reinforcement in the normal direction while in the tangential direction, slip occurs. In contact elements, the normal stiffness of the interface is given very high value to prevent interpenetration of nodes.

✉ V. B. Maji
vbmaji@gmail.com

[1] Department of Civil Engineering, Indian Institute of Technology Madras, Chennai, India

Good amount of literature is available in modelling reinforced soils using numerical approaches like Karpurapu and Bathurst [1], Nakane et al. [2], Rowe and Ho [3], Leshchinsky and Vulova [4], Ling and Leshchinsky [5] and Yoo and Song [6], Hatami and Bathurst [7, 8], Guler et al. [9] amongst many others. Ling and Leshchinsky [5], Hatami and Bathurst [7, 8] and Guler et al. [9] verified their numerical models against carefully constructed, instrumented and monitored walls. Reviews of numerical modelling of geosynthetic reinforced soil wall can be found in the papers by Bathurst and Hatami [10] and Ling [11]. Guler et al. [9] studied the failure mechanisms of reinforced segmental walls by finite element (FE) analysis and later Bergado and Teerawattanasuk [12] carried out numerical simulations of steel grid reinforced long embankments using finite difference method (FDM) based software, *FLAC* and *FLAC*[3D]. Bathurst et al. [13] studied the effect of constitutive models on the response of two full scale reinforced soil walls during construction and surcharge loading. Gerrard and Harrison [14] used equivalent homogenizing material concept and the material properties including system of alternating isotropic layers of earth and a set of parallel equally spaced reinforcing meshes were defined. Romstad et al. [15] used composite stress concept and defined the properties of orthorhombic material. Boyle [16] developed an analytical model and treated the geosynthetic reinforced soil as composite material by adopting transversely isotropic homogenous material concept. Chen et al. [17] approached the reinforced soil as a homogenized soil model using a transversely isotropic concept. Yammamoto and Otani [18] used Drucker–Prager model for reinforced sand and the reinforcement effect is included by introducing pseudo cohesion c_R [19].

Present study uses the equivalent approach to develop a numerical model using *FLAC*, considering the reinforced soil as homogeneous material. The model is verified with large diameter triaxial tests conducted in the laboratory with different types of reinforcements. To demonstrate the applicability and simplicity of the model, analysis is carried out for two case studies from the literature, a full scale geogrid reinforced retaining wall constructed at Royal Military College of Canada (RMC) [20] and a reinforced retaining wall problem [9]. The effectiveness and capability of the equivalent numerical analysis is systematically verified by comparing with the instrumented data and also with discrete model where the reinforcements were explicitly modelled.

Experimental Studies

A series of triaxial tests were performed on unreinforced and reinforced soil samples at different relative densities and confining pressures. Different reinforcing elements such as a grey mesh (GM), yellow mesh (YM), fishing net (FN) and woven geotextile (WGT) were selected (Fig. 1). River sand was chosen for the current study and is classified as poorly graded sand (SP). The properties of sand obtained from the laboratory tests are summarized in Table 1.

The tensile strength of the reinforcing elements were determined as per ASTM D4595-11. This tests were performed by either wide width tests (200 mm wide) or narrow strip tests (50 mm wide) (Fig. 2). In the current research work, narrow strips of reinforcements were considered for testing. Wide width test was considered for Fishing Net, since its aperture opening size is relatively large compared to other samples. The reinforcement strips were gripped across its entire width in the clamps of the constant rate of extension (CRE) type tensile testing machine (roller grips) and load was applied at the rate of 10–20 % strain per minute. Table 2 summarizes the properties of the reinforcing elements.

Direct shear tests were conducted to study the shear strength parameters of unreinforced sand. Three normal stresses of 50, 100 and 200 kPa were used. The samples were prepared at three relative densities of 40, 60 and 80 %. A total of nine direct shear tests on unreinforced sand were carried out.

Standard triaxial compression tests were conducted on samples of 100 mm diameter and 200 mm height on both unreinforced and reinforced dry samples. The test setup is shown in Fig. 3. A total of 53 triaxial tests were conducted to understand their mechanical behavior. For all the tests, a deformation rate of 0.125 mm/min was adopted [21]. The stress–strain behaviour of unreinforced and reinforced soil at different confining pressures and relative densities were investigated. Typical stress–strain results for relative density of 60 % and confining pressure of 100 kPa are shown in Fig. 5. The reinforced soil resulted in increased peak strength, axial strain at failure and reduction in post peak loss. These data were used to validate the numerical model. Direct shear pullout test was conducted to get the interface properties and the setup is shown in Fig. 4.

Numerical Model

Numerical Model for reinforced soil was developed using *FLAC* [22] using equivalent approach and validated with laboratory triaxial tests. Two basic constitutive models such as the Mohr–Coulomb elastic–plastic model (MC) and the Duncan–Chang (DC) hyperbolic model [23] were used. *FLAC* with axisymmetry geometry is used to simulate the reinforced sand based on equivalent approach and all the model parameters were determined from the laboratory tests. A *FLAC*[3D] model to simulate triaxial test on

Fig. 1 Types of reinforcing elements used **a** grey mesh (GM), **b** yellow mesh (YM), **c** fishing net (FN), and **d** woven geotextile (WGT). (Color figure online)
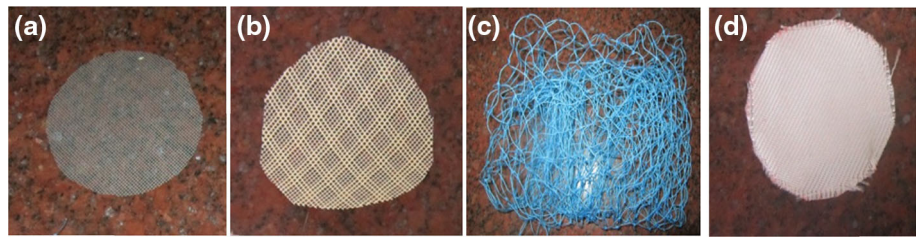
Table 1 Properties of sand used for the study

Sl. no.	Property	Values
1	Specific gravity	2.67
2	D_{50} (mm)	1
3	D_{60} (mm)	1.3
4	D_{30} (mm)	0.6
5	D_{10} (mm)	0.3
6	C_u	4
7	C_c	1
8	Maximum unit weight (kN/m^3)	17.5
9	Minimum unit weight (kN/m^3)	14.9

reinforced sand based on discrete approach was also developed. Table 3 gives the summary of Mohr–Coulomb soil parameters derived from triaxial stress–strain curves and Table 4 gives the summary of hyperbolic parameters

derived from triaxial stress–strain curves. The hyperolic model expression [23] for instantaneous slope of the stress strain curve, the tangent modulus 'E_t' is given by the following Eq. 1.

$$E_t = \left[1 - \frac{R_f (1 - \sin \phi)(\sigma_1 - \sigma_3)}{2c \cos \phi + 2\sigma_3 \sin \phi} \right]^2 K \cdot p_a \left(\frac{\sigma_3}{p_a} \right)^n \quad (1)$$

The equation was used to calculate the approximate value of tangent modulus for any stress condition 'σ_3' and $(\sigma_1 - \sigma_3)$ for the known values of the parameters, modulus number (K), modulus exponent (n), cohesion (c), angle of internal friction (ϕ), failure ratio (R_f) and p_a represents the atmospheric pressure. The bulk modulus of the soil can be expressed as,

$$B = K_b \cdot p_a \left(\frac{\sigma_3}{p_a} \right)^m \quad (2)$$

where K_b and m are bulk modulus number and bulk modulus exponent respectively. The tangent Poisson's ratio (v_t)

Fig. 2 Typical failure of the reinforcing elements during tensile strength test

Table 2 Properties of reinforcing elements

S. no.	Reinforcement type	Nominal thickness (mm)	Aperture opening size (mm)	Max. tensile strength (kN/m)		Max. elongation (%)	
				LD	TD	LD	TD
1	GM	0.2	1.5	4.4	4.3	5	5
2	YM	0.3	1.5	1.6	1.5	83	75
3	FN	1	25	2.2	2	12	12
4	WGT	1	NA	55.4	32	4.4	3.4

LD longitudinal direction, *TD* transverse direction

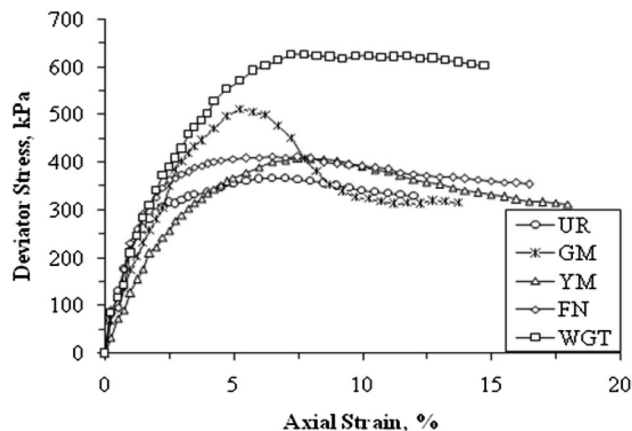Fig. 3 Triaxial testing with loading frame and large scale triaxial cell

Fig. 5 The stress–strain curves for unreinforced and reinforced sand at RD-60 % and at confining pressures of 100 kPa

of reinforcement-soil interface, i.e. interaction between the geogridSEL elements with that of the surrounding soil model, is controlled by three coupling spring properties such as coupling spring cohesion (cs_scoh), friction (cs_sfric) and stiffness (cs_k). These interface properties can be obtained from pull-out tests performed at different normal loads in the laboratory. The stiffness (cs_k) corresponds to the slope of the pull-out stress versus displacement plot which increases with increasing confinement. The values of cohesion (cs_scoh) and friction (cs_sfric) were obtained from a plot of maximum pull out force versus confinement. The slope of this curve corresponds to friction (cs_sfric) and the y-intercept equals to cohesion (cs_scoh). Thus interface stiffness is expressed as following.

$$\text{cs\_k} = \frac{\Delta S}{\Delta U} \quad \left(\text{N/m}^2/\text{m}\right) \tag{3}$$

where S is the Pullout stress (Pull out force/embedded area) (N/m^2) and U is the Pullout displacement (m).

The interface properties determined from pull out test data for different reinforcing elements are given in Table 6. From Table 6, it is clear that the interface friction obtained by the above procedure is relatively low for all the reinforcing elements. The interface friction obtained is found to very low for all the reinforcing elements and the adhesion values appears to be very high. This is because the friction obtained due to pull out is only apparent. The higher value of adhesion may be due to interlocking of material, which adds up to the interface adhesion and the passive bearing against the transverse members of the geosynthetics.

The stress–strain responses were predicted numerically, by executing the *FISH* functions in *FLAC*. The numerical
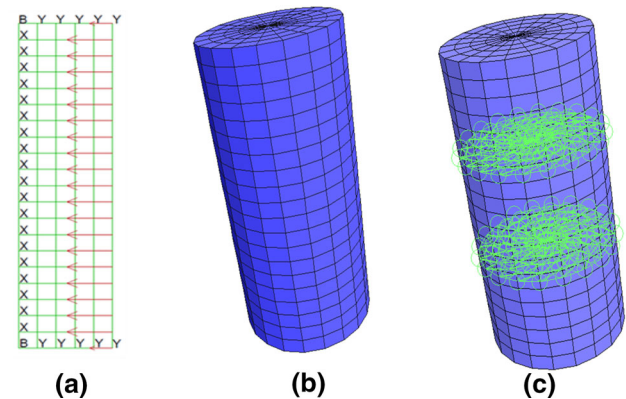

Fig. 4 The direct shear pull out test setup

can be calculated using elasticity theory. Numerical grids for unreinforced and reinforced soil samples are shown in Fig. 6. Figure 6a shows the axi-symmetric *FLAC* grid whereas Fig. 6b–c represents the *FLAC*^{3D} zones for equivalent and discrete model, respectively. The reinforcement layers are modelled using geogridSEL [24] structural elements whose properties are summarized in Table 5. The interface between the reinforcement and soil are simulated by coupling spring properties which are shown in Table 6. For discrete approach, the interface elements in *FLAC*^{3D} are used to simulate the contacts between soil and the reinforcements. The shear behaviour

Table 3 Summary of Mohr–Coulomb soil parameters derived from triaxial tests

Test condition σ_3 (kPa)	RD-40 %			RD-60 %			RD-80 %		
	E_i (kPa)	c (kPa)	$\phi°$	E_i (kPa)	c (kPa)	$\phi°$	E_i (kPa)	c (kPa)	$\phi°$
Unreinforced									
50	13,600	7.6	36	15700	14.4	37	17,800	14.3	39.64
100	17,600			21,600			25,600		
200	25,000			29,400			37,600		
Reinforced (GM)									
50	10,200	52.5	35.5	11,200	44.2	37.52	12,200	83.4	36
100	11,900			13,400			18,800		
200	12,540			14,800			27,400		
Reinforced (YM)									
50	9000	27.3	36.9	10,200	40.6	35.45	10,400	25.8	39.56
100	10,000			11,400			11,200		
200	19,000			22,000			20,200		
Reinforced (FN)									
50	4200	28.4	35.2	9800	28.9	37.5	15,400	23.2	39.2
100	11,000			17,600			24,000		
200	26,800			29,600			33,500		
Reinforced (WGT)									
50	12,000	33.5	41.4	15,400	32	43.3	18,000	68.8	43
100	13,000			17,800			26,200		
200	19,400			29,600			33,500		

Table 4 Duncan–Cheng hyperbolic parameters derived from triaxial tests

Soil type	Hyperbolic parameters		
	K	n	R_f
Unreinforced soil	75–100	0.6	0.75
Reinforced soil			
Grey mesh (GM)	160–200	0.5	0.8
Yellow mesh (YM)	250–300	0.5	0.8
Fishing net (FN)	400	0.6	0.8
Woven geotextile (WGT)	900	0.6	0.8

Fig. 6 **a** *FLAC* mesh of reinforced (equivalent) triaxial soil sample (axi-symmetric), **b** *FLAC*^{3D} zones for unreinforced soil sample, and **c** reinforced soil sample (discrete approach)

experiments were repeated for different confining pressures and different relative densities, very similar to laboratory triaxial tests. Figures 7, 8 and 9 show typical stress–strain curves of reinforced soil, based on equivalent and discrete approaches. Both the approaches yield comparable results with slightly underestimation of axial strain values at failure. Figure 7 compares the stress–strain curves of GM reinforced sand (RD-40 %, σ_3-50 kPa) obtained using equivalent approach using MC model with experimental data. Comparison of stress–strain curves of WGT

Table 5 Reinforcement properties

Reinforcement type	E (kPa)	v (assumed)	Thickness (m)
Grey mesh	8.0×10^5	0.35	0.0002
Yellow mesh	2.88×10^4	0.35	0.0005
Fishing net	6.0×10^4	0.35	0.0005
Woven geotextile	1.7×10^6	0.35	0.0005

Table 6 Soil–reinforcement interface properties derived from pull out tests

Reinforcement type	Relative density (%)	Stiffness, cs_k (N/m²/m) (×10⁷)			Adhesion (cs_scoh) (kPa)	Friction (cs_sfric) (°)
		$\sigma_v = 60$ kPa	$\sigma_v = 100$ kPa	$\sigma_v = 210$ kPa		
GM	40	0.808	0.789	0.852	14.810	2.64
	60	0.900	0.768	0.882	20.070	2.75
	80	0.903	0.980	0.113	20.050	6.00
YM	40	0.467	0.325	0.447	7.246	3.03
	60	0.292	0.409	0.519	9.063	2.97
	80	0.395	0.463	0.459	12.280	2.80
WGT	40	1.230	1.370	1.560	42.850	5.88
	60	1.390	1.670	1.710	45.780	7.35
	80	1.500	1.720	1.660	50.500	7.35
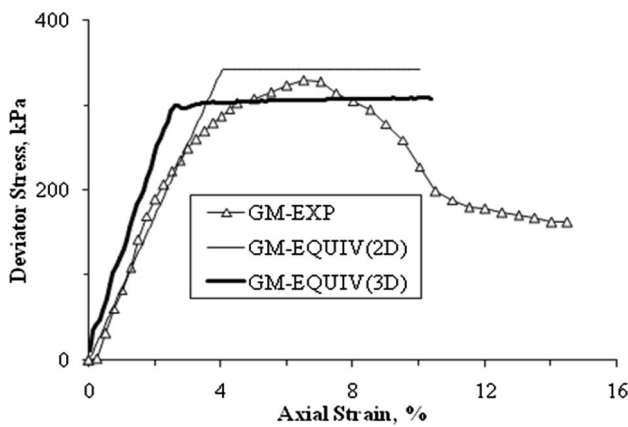
Fig. 7 Comparisons of stress–strain curves of GM reinforced sand (RD-40 %, σ_3-50 kPa) using equivalent approach for MC model
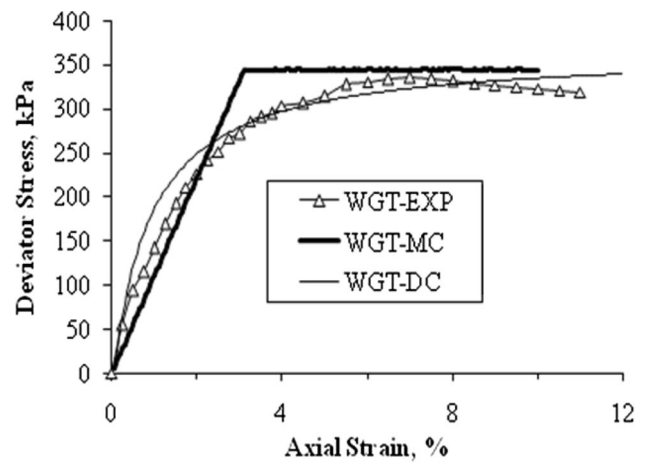
Fig. 9 Comparisons of stress–strain curves of WGT reinforced sand (RD-40 %, σ_3-50 kPa) using Mohr–Coulomb and Duncan–Chang model
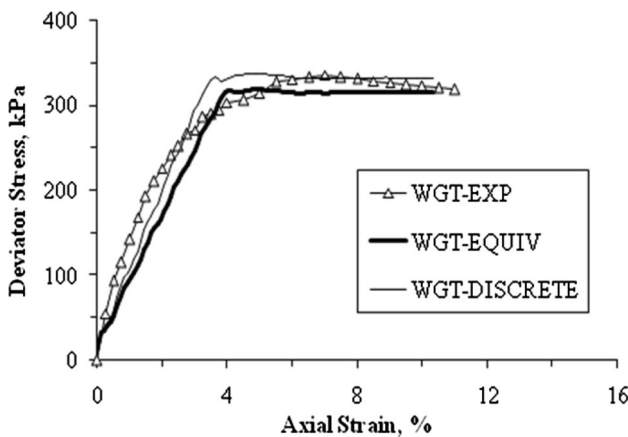
Fig. 8 Comparison of stress–strain curves of WGT reinforced sand (RD-40 %, σ_3-50 kPa) based on equivalent and discrete approach

reinforced sand (RD-40 %, σ_3-50 kPa) obtained using $FLAC^{3D}$ based on equivalent approach and discrete approach with experiments are shown in Fig. 8. Figure 9 compares the stress–strain curves of WGT reinforced sand (RD-40 %, σ_3-50 kPa) using equivalent approach with the experiments. It is observed that the stress–strain curves based on equivalent approach are in close agreement with that of experimental data and is able to predict the stress–strain response quite well up to the peak.

Case Studies

Guided by the analysis of triaxial testing results, the applicability of equivalent approach is evaluated by analysing two case studies. A reported case study on a full

scale geogrid reinforced retaining wall constructed at Royal Military College of Canada (RMC) [7, 8] and a reinforced retaining wall problem analysed by Guler et al. [9] were analysed using *FLAC*. The equivalent numerical model is systematically verified with the instrumented data together with results from discrete approach.

Full Scale Reinforced Test Wall

A reinforced soil retaining wall was analysed to study the deformation behaviour of the structure. Full scale reinforced retaining test walls were constructed at the Royal Military College of Canada (RMCC) in a long term research project [20]. In total, eleven full scale reinforced retaining walls were carefully constructed, instrumented and monitored. Out of which, one reinforced segmental wall (wall 1, with 6 layers of polypropylene, [7] structure is considered in the present study. The wall was 3.6 m high with a target facing batter of 8° to the vertical. The length of the backfill was about 6 m. This wall was constructed with 2.52 m long biaxial polypropylene geogrid and had 0.6 m vertical spacing between the reinforcement layers. Modular blocks, of 300 mm long, 200 mm wide and 150 mm high, weighing 196 N were used. The dimension of the full scale test wall is shown in Fig. 10.

The model parameters were taken same as that of the data reported by Hatami and Bathurst [7] where the actual test walls were verified numerically using *FLAC* using discrete approach. The same wall is modelled in the current study using equivalent approach. A large scale triaxial test was first numerically simulated by using the soil and reinforcement properties available in the literature and the equivalent parameters are then determined from the numerically obtained triaxial stress strain curves. These equivalent parameters are then used in the analysis of reinforced retaining wall, where the parameters in the reinforced zone (up to reinforcement length) are replaced by the equivalent parameters. Large scale triaxial sample of length to diameter ratio 2:1 representing the test wall is
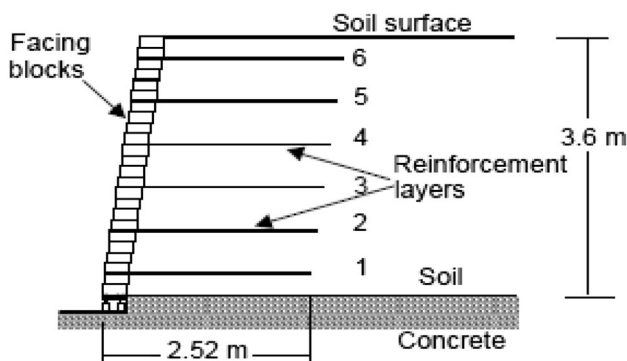
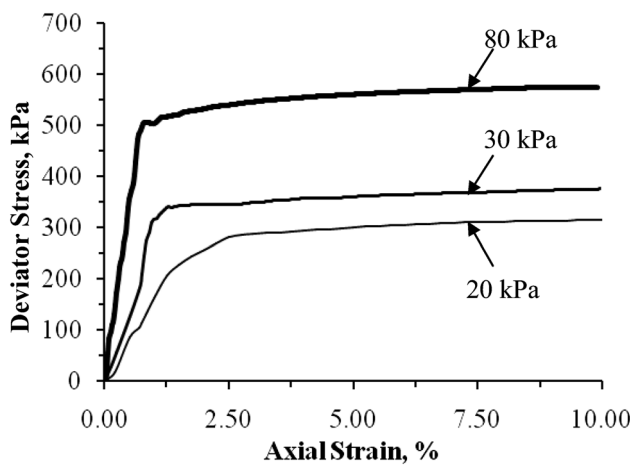Fig. 10 Model geometry and components of full scale segmental test wall [7]
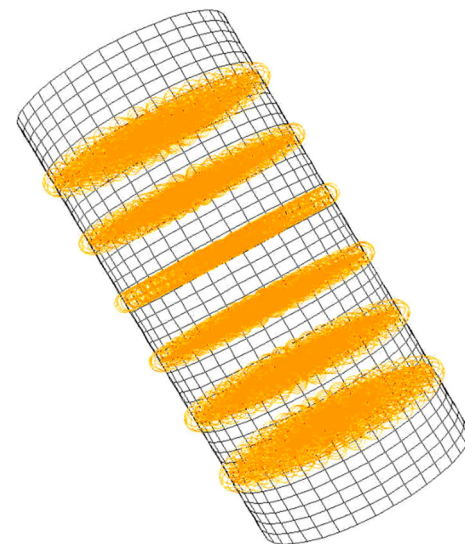
Fig. 11 Numerical simulation of reinforced triaxial sample

numerically simulated based on discrete approach and is shown in Fig. 11. The sample is reinforced with 6 layers of biaxial polypropylene geogrid with 60 cm vertical spacing in order to simulate the field conditions. Table 7 gives the summary of soil and reinforcement properties adopted from the literature to simulate the triaxial test. The stress–strain curves obtained from the numerical simulation of triaxial tests at various confining pressures are shown in Fig. 12. Table 8 gives the summary of equivalent parameters derived from numerical triaxial tests. The hyperbolic equivalent parameters are obtained from the best fit hyperbolic curves. Figure 13 shows different trials of Duncan–Cheng hyperbolic curves that match well with the Mohr–Coulomb stress–strain curves. The parameters of the best fit hyperbolic curves are taken as equivalent hyperbolic parameters and are summarized in Table 8. Table 9 summarizes the model parameters used for the retaining wall beyond the reinforcement portion adopted from Hatami and Bathurst RJ [7].

The equivalent model parameters determined from the numerical triaxial tests and the backfill soil properties obtained from the literature are substituted for analysis with equivalent soil and backfill soil, respectively. The modular blocks are modeled as linear elastic units and their properties are taken from the literature. The construction of the wall was modelled by bottom up approach where soil layers of 0.15 m thick (height of each modular block) were placed sequentially up to the final wall height. The compaction of each layer of soil is simulated by applying a distributed load of 8 kPa at every lift using beam elements [7]. The weight of the beam element was taken as 8 kN/m with very small axial stiffness and flexural rigidity to avoid any strength contribution. After the construction phase was complete,

Table 7 Soil and reinforcement properties used for triaxial test simulation [7]

Property	Values
Soil	
Unit weight γ (kN/m³)	16.8
Young's modulus E (MPa)	
$\sigma_3 = 20$ kPa	10.24
$\sigma_3 = 30$ kPa	15
$\sigma_3 = 80$ kPa	26
Friction angle ϕ (°)	44
Dilation angle ψ (°)	11
Cohesion c (kPa)	0.2
Reinforcement (biaxial polypropylene geogrid) axial stiffness (kN/m)	97
Interface (soil–reinforcement)	
Interface friction angle ϕ_b (°)	44
Adhesive strength (kPa)	1000
Shear stiffness (kN/m/m)	1000

Fig. 12 Stress–strain curves obtained from numerically simulated reinforced triaxial tests

Table 8 Summary of equivalent parameters

Mohr–Coulomb parameters	
Unit weight γ (kN/m³)	16.8
Young's Modulus E (MPa)	
$\sigma_3 = 20$ kPa	12
$\sigma_3 = 30$ kPa	34
$\sigma_3 = 80$ kPa	70
Triaxial friction angle ϕ (°)	36.5
Cohesion c (kPa)	70
Duncan–Chang hyperbolic parameters	
K	
$\sigma_3 = 20$ kPa	1000
$\sigma_3 = 30$ kPa	1400
$\sigma_3 = 80$ kPa	4000
n	0.6
R_f	0.80

surcharge pressures were applied in 10 kPa increments. Figure 14 shows the *FLAC* numerical grid of the equivalent full scale retaining wall. In the *FLAC* model, separate colours are prescribed to distinguish the facing elements, zones containing the geo-synthetic reinforcement (as equivalent model) and soil beyond the reinforcement zones. In the numerical analysis, the horizontal facing displacements were determined from the nodes at the facing elements which are at the same level with the reinforcement. Table 10, gives the summary of both the model predictions together with discrete element results and are found to be in close agreement with the measured data reported in the literature. From Table 10, it is seen here that the Mohr–Coulomb model yielded slightly higher prediction of facing displacement at the end of construction than hyperbolic model. In the present case, Mohr–Coulomb model appears to give better estimate of

wall deformation than Duncan–Chang Hyperbolic model and is in consistent with that of reported values [7, 8].

Reinforced Retaining Wall

The retaining wall model geometry and dimensions adopted from the literature [9] is shown in Fig. 15. The wall height is 9 m and the width of the backfill zone is 25 m. The facing elements are made with modular blocks of 50 cm width and 25 cm height. The length of the reinforcement (L) is 4.5 m which correspond to L/H ratio of 0.5, where, H is the total height of the retaining wall (9 m).
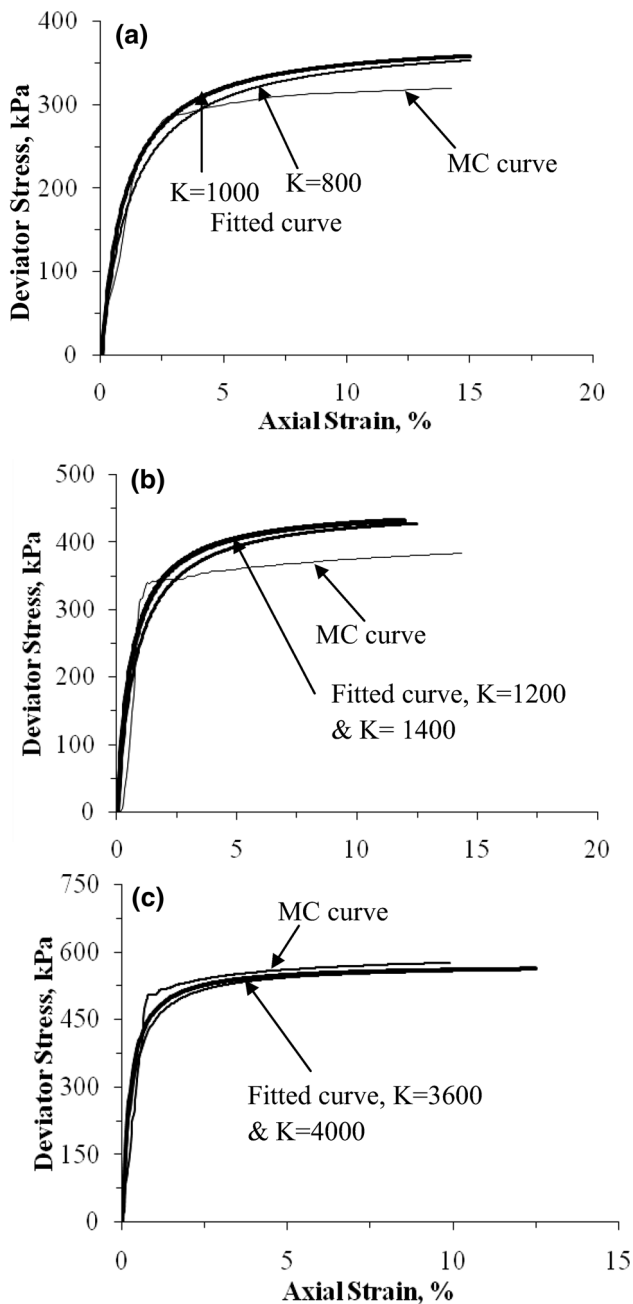
Fig. 13 Different trials of hyperbolic curves with σ_3 of **a** 20, **b** 30 and **c** 80 kPa

The spacing of the reinforcement layers is 1 m. The properties of soil, reinforcement, modular blocks and interface are taken from the literature [9].

The retaining wall is modeled with both discrete and equivalent approaches and the analysis was done in two phases. The first phase includes wall construction and the second phase includes c–ϕ reduction analysis to study the failure mechanism and to determine the safety factor. The soil is modelled as linear elastic–plastic material using Mohr–Coulomb model where as reinforcement layers are

Table 9 Model parameters used for the retaining wall beyond the reinforcement portion [7]

Backfill soil (Mohr–Coulomb Model)	
Unit weight γ (kN/m^3)	16.8
Young's modulus E (MPa)	40
Friction angle ϕ (°)	44
Dilation angle ψ (°)	11
Cohesion c (kPa)	0.2
Backfill soil (hyperbolic model)	
Elastic modulus number (K)	800
Failure ratio (R_f)	0.86
Modulus exponent (n)	0.5
Interface between modular block and backfill soil	
Interface friction angle ϕ_b (°)	44
Dilation angle ψ_b (°)	11
Normal stiffness (MN/m/m)	100
Shear stiffness (MN/m/m)	1

modelled as cable elements. The interface at the facing column-backfill, reinforcement-backfill were modelled as linear spring-slider systems with interface shear strength defined by Mohr–Coulomb failure criterion.

In the equivalent approach, the cohesion in the reinforced zone (up to the length of reinforcement) is increased using pseudo cohesion or anisotropic cohesion concept [19]. The reinforced soil fails at a higher vertical stress level and the additional strength was imparted by an apparent anisotropic cohesion (c). For the present study, the value of cohesion was found to be 70 kPa after performing many trials. Thus in the equivalent approach, each soil lift consists of placing the modular blocks, backfill equivalent reinforced soil layer up to 4.5 m (length of reinforcement) whose equivalent cohesion is 70 kPa and placing of the backfill soil layer. Each soil layer is then subjected to self weight at each lift. The same process was repeated till the full wall height was reached. At the end of construction, the wall was subjected to initial equilibrium and then c–ϕ reduction analysis was carried out to find out the safety factor. Table 11 gives the summary of material properties taken from the literature and also the equivalent cohesion used in the current study. For discrete approach, the soil and reinforcement properties and the interface properties [9] are also given in Table 11. Figure 16a, b show the *FLAC* numerical grid of reinforced retaining wall based on equivalent and discrete approaches respectively.

Figure 17a, b show the maximum shear strain increments at the end of construction for both discrete and

Fig. 14 *FLAC* numerical grid of equivalent full scale retaining wall
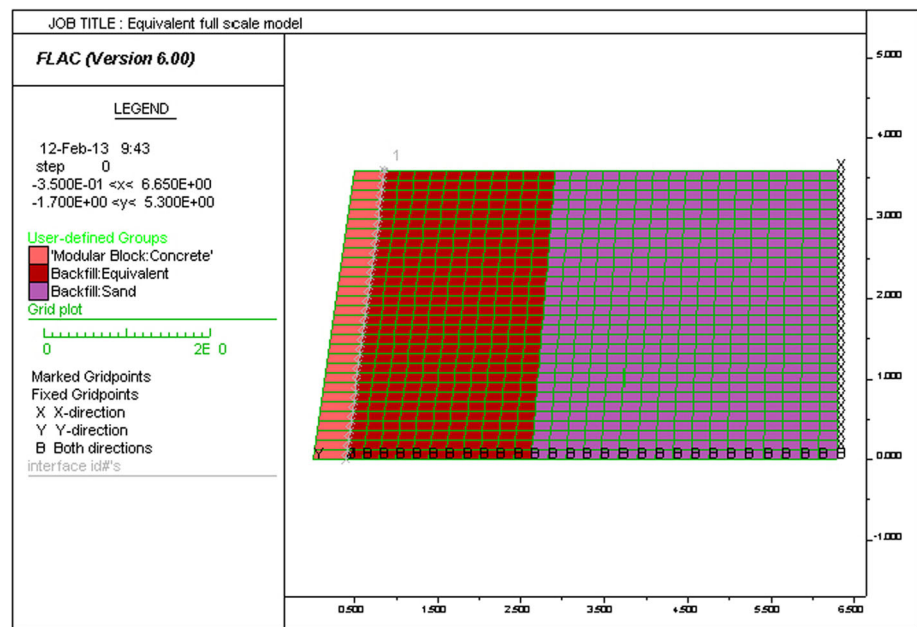
Table 10 Summary of facing displacements at different conditions

Condition	Maximum facing displacement (mm)				
	During construction	During surcharging			
		40 kPa	50 kPa	60 kPa	70 kPa
Instrumented [7, 8]	6–7	10–12	18–20	24–26	34–36
Discrete model [7, 8]	5–6	9–11	16–18	20–22	28–30
Equivalent model					
MC model	6–7	10–11	15–16	20–22	30–31
DC model	4–5	7–8	14–15	22–24	33–35
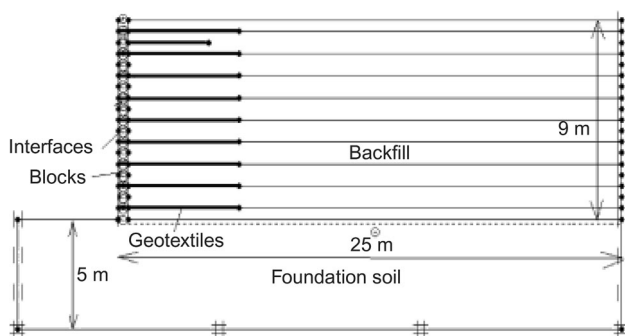
Fig. 15 The model geometry and dimensions of reinforced retaining wall [9]

Table 11 Reinforced retaining wall properties [9]

Soil properties	
Unit weight γ (kN/m^3)	20
Young's modulus E (kPa)	30,000
Friction angle ϕ (°)	35
Cohesion c (kPa)	5
Modular blocks	
Young's modulus E (kPa)	50,000
Cohesion c (kPa)	200
Friction angle ϕ (°)	35
Reinforcement biaxial polypropylene geogrid	
Elastic axial stiffness (kN/m)	1500
Interface (modular block)	
Interface friction angle ϕ_b (°)	35
Adhesive strength (kPa)	5

equivalent approaches. The maximum shear strain concentration is linear and is inclined with the horizontal. This shear strain concentration represents the failure surface and is reasonably close to the assumed failure surface in the conventional design [inclined at $(45° + \phi/2)$]. Figure 18a, b show the maximum shear strain increments at the end of c–ϕ

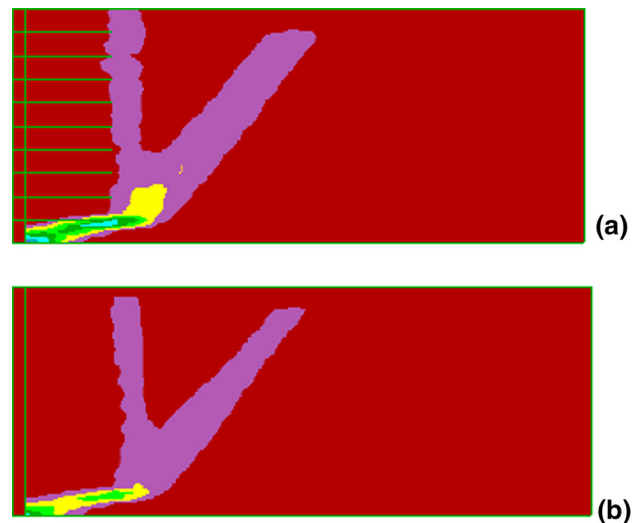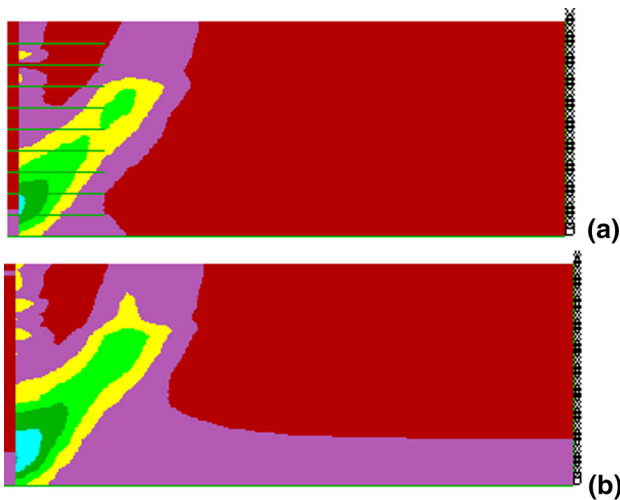reduction analysis for both discrete and equivalent approaches. At the end of c–ϕ reduction analysis, the ultimate failure line is changed to bilinear failure plane, which shows
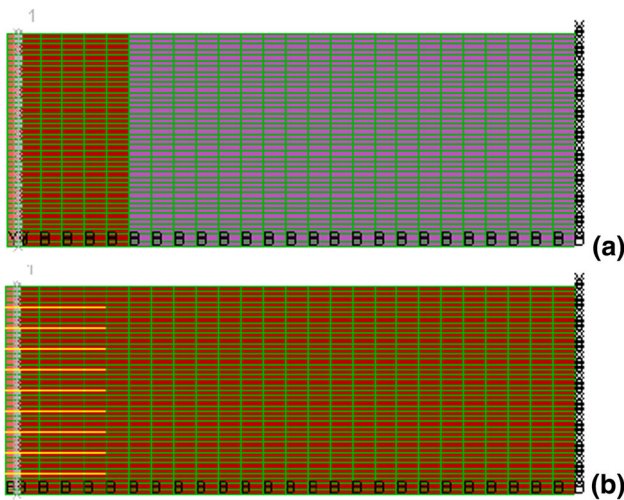
Fig. 16 *FLAC* numerical grid of reinforced retaining wall based on **a** discrete approach and **b** equivalent approach

Fig. 17 Maximum shear strain increment at the end of construction **a** discrete approach and **b** equivalent approach

a direct sliding mode [9]. In this case, the internal failure mechanism is not critical as the shear strain concentration is away from the reinforced soil zone and the equivalent approach could be used for the analysis purpose. Table 12 shows the summary of the *FLAC* results at the end of c–ϕ analysis. The factor of safety values from the equivalent approach is in good agreement with that of the values reported in the literature and also with the discrete approach.

Conclusions

An attempt is made to analyse reinforced soil with equivalent approach by carrying out experimental and numerical studies. To study the reinforced soil behaviour, triaxial tests with large diameter cell were carried out in the laboratory

Fig. 18 Maximum shear strain increment at the end of c–ϕ reduction analysis **a** discrete approach and **b** equivalent approach

Table 12 Summary of *FLAC* analysis results

Model type	Factor of safety
Discrete approach	1.80
Equivalent approach	1.69
Literature [9]	1.76

such that the overall behaviour of the reinforced sand could be studied. Numerical simulations of the laboratory triaxial tests were carried out using *FLAC* code and a model for the reinforced sand based on equivalent material approach is developed. The input parameters for the numerical model were derived directly from the laboratory triaxial tests. The model uses Mohr–Coulomb elasto plastic model and non-linear hyperbolic model with systematic verification of the results against the experimental data. Model is also compared with discrete model where the reinforcement layers are explicitly modelled. The developed equivalent model could capture the strength and deformation behaviour of the reinforced sand and the failure mechanisms. The hyperbolic model is found to be efficient in capturing the non-linear stress–strain response of reinforced soil up to the peak. To extend the applicability of the model, model was applied to two reported case studies. The model could capture the behavior well and the approach can be used to study the overall behaviour of the reinforced soil structures.

References

1. Karpurapu RG, Bathurst RJ (1995) Behaviour of geosynthetic reinforced soil retaining walls using the finite element method. Comput Geotech 17(3):279–299

2. Nakane A, Yokota, Y, Taki, M, Miyatake H (1996) FEM comparative analysis of facing rigidity of geotextile reinforced soil walls. In: Ochiai H, Yasufuku N, Omine K (eds) Proceedings of the international symposium on earth reinforcement, Fukuoka, Kyushu, Japan, 12–14 Nov. AA Balkema, Rotterdam,pp 433–438

3. Rowe RK, Ho SK (1997) Continuous panel reinforced soil walls on rigid foundations. J Geotech Geoenviron Eng 123(10): 912–920

4. Leshchinsky D, Vulova C (2001) Numerical investigation of the effects of geosynthetic spacing on failure mechanisms in MSE block walls. Geosynth Int 8(4):343–365

5. Ling HI, Leshchinsky D (2003) FE parametric study of the behavior of segmental block reinforced-soil retaining walls. Geosynth Int 10(3):77–94

6. Yoo S, Song AR (2006) Effect of foundation yielding on performance of two-tier geosynthetic-reinforced segmental retaining walls: a numerical investigation. Geosynth Int 13(5):181–194

7. Hatami K, Bathurst RJ (2005) Development and verification of a numerical model for the analysis of geosynthetic-reinforced soil segmental walls under working stress conditions. Can Geotech J 42(4):1066–1085

8. Hatami K, Bathurst RJ (2006) Numerical model for reinforced soil segmental walls under surcharge loading. J Geotech Geoenviron Eng ASCE 132(6):673–684

9. Guler E, Hamderi M, Demirkan MM (2007) Numerical analysis of reinforced soil-retaining wall structures with cohesive and granular backfills. Geosynth Int 14(6):330–345

10. Bathurst RJ, Hatami K (2001) Review of numerical modeling of geosynthetic reinforced soil walls. In: Invited theme paper, computer methods and advances in geomechanics: 10th international conference of the international association for computer methods and advances in geomechanics, 7–12 January 2001, Tucson, Arizona, vol 2, pp 1223–1232

11. Ling HI (2003) Finite element applications to reinforced soil retaining walls–simplistic versus sophisticated analyses. In: Yamamuro JA, Koseki J (eds) Geomechanics: testing, modeling and simulation, 1st Japan–U.S. workshop on testing, modeling, and simulation. ASCE geotechnical special publication no. 143, Boston, pp 77–94

12. Bergado DT, Teerawattanasuk C (2008) 2D and 3D numerical simulations of reinforced embankments on soft ground. Geotext Geomembr 26(1):39–55

13. Bathurst RJ, Huang B, Hatami K (2009) Numerical study of Reinforced soil segmental walls using three different constitutive soil models. J Geotech Geoenviron Eng ASCE 135(10): 1496–1498

14. Gerrard CM, Harrison WJ (1972) Elastic theory applied to reinforced earth. J Soil Mech Found Div ASCE 98(12):1325–1345

15. Romstad KM, Herrmann LR, Shen CK (1976) Integrated study of reinforced earth-I: theoretical formulation. J Geotech Eng ASCE 102(5):457–472

16. Boyle SR, Gallagher M, Holtz RD (1996) Influence of strain rate, specimen length and confinement on measured geotextile properties. Geosynth Int 3(2):205–225

17. Chen RH, Chen TC, Lin SS (2000) A nonlinear homogenized model applicable to reinforced soil analysis. Geotext Geomembr 18:349–366

18. Yamamoto K, Otani J (2002) Bearing capacity and failure mechanism of reinforced foundations based on rigid-plastic finite element formulation. Geotext Geomembr 20(6):367–393

19. Chapius (1972) Rapport de recherchė de DEA. Institu de Mecanique de Grenoble

20. Bathurst RJ, Walters D, Vlachopoulos N, Burgess P Allen TM (2000) Full scale testing of geosynthetic reinforced walls. ASCE special publication no 103. Advances in transportation and geoenvironmental systems using geosynthetics. Proceedings of Geo-Denver 2000. Invited keynote paper, pp 201–217

21. Sowmiya VS (2013) Equivalent material approach to reinforced soil. MS Thesis, Department of Civil Engineering. Indian Institute of Technology Madras, Chennai, India

22. Itasca Consulting Group Inc (1999) Fast Lagrangian analysis of continua. *FLAC* version 4, User's manuals

23. Duncan JM, Chang CY (1970) Non-linear analysis of stress and strain in soil. J Soil Mech Found Eng ASCE 5:1629–1652

24. Itasca Consulting Group Inc (2001) Fast Lagrangian analysis of continua in 3-dimesions. *FLAC^{3D}* version 2.1, User's manuals